Charge Asymmetry in the Decay $K_L^0 \to \pi\mu\nu$

R. L. McCarthy,* J. H. Brewer, R. J. Budnitz, A. C. Entis,†
R. M. Graven, D. H. Miller,‡ and W. N. Ross§

Lawrence Berkeley Laboratory, University of California, Berkeley, California 94720

(Received 31 July 1972)

If $\Gamma_\pm = \text{Rate}(K_L^0 \to \pi^\mp \mu^\pm \nu)$, the $K_{\mu 3}^0$ charge asymmetry is $\delta = (\Gamma_+ - \Gamma_-)/(\Gamma_+ + \Gamma_-)$. This number has been measured to be $(6.0 \pm 1.4) \times 10^{-3}$ at the Lawrence Berkeley Laboratory's Bevatron. The error is meant to be interpreted as one standard deviation and contains a major systematic contribution. Large corrections were made in order to exclude neutron-induced background events and to correct for the range difference between μ^+ and μ^-. The meaning of the possible difference between muonic and electronic charge asymmetries is discussed.

I. INTRODUCTION

The charge asymmetries in the semileptonic decays $K_L^0 \to \pi^\mp l^\pm \nu$ are the only known manifestations of CP violation aside from the decays $K_L^0 \to \pi\pi$. Assuming CPT invariance and that the semileptonic decays proceed by first-order weak interactions only,[1] it is possible to relate the charge asymmetries to ϵ, the CP mixture parameter of the neutral-K-meson states, and to x_l, the $\Delta S = \Delta Q$ violation parameter[2]:

$$\delta_l = (\Gamma_+ - \Gamma_-)/(\Gamma_+ + \Gamma_-)$$
$$= 2\,\text{Re}\,\epsilon F_l \ ,$$
$$F_l = (1 - |x_l|^2)/|1 - x_l|^2.$$

Here $\Gamma_\pm$ is the rate for decay to $\pi^\mp l^\pm \nu$ (l is either a muon or an electron). If the $\Delta S = \Delta Q$ rule holds in weak interactions, F_l is equal to 1 and $\text{Re}\,\epsilon = \frac{1}{2}\delta_l$.

The study of the $K_{\mu 3}^0$ charge asymmetry separately from the K_{e3}^0 charge asymmetry is interesting for two reasons. First, the measurement techniques and hence the sources of possible systematic errors are quite different in the two cases; second, owing to the factor F_l, the two charge asymmetries can differ. Such a difference would *not* necessarily violate μ-e universality because F_l could depend on the lepton mass, for example, through the well-known presence of the f_- form factor, which is important only in the $K_{\mu 3}^0$ decay. A difference of F_l from unity would, however, necessarily indicate a violation of the $\Delta S = \Delta Q$ rule.

We report a new measurement of the muonic charge asymmetry.[3] The result of this experiment should be compared to the previous result for the $K_{\mu 3}^0$ asymmetry,[4] the best value of the K_{e3}^0 asymmetry,[5] and the prediction of the superweak

theory[6]:

this experiment	$\delta_\mu = (6.0 \pm 1.4) \times 10^{-3}$,
previous $K_{\mu 3}^0$	$\delta_\mu = (5.7 \pm 1.7) \times 10^{-3}$,
best value K_{e3}^0	$\delta_e = (3.22 \pm 0.29) \times 10^{-3}$,
superweak theory	$\delta = (2.80 \pm 0.08) \times 10^{-3}$.

The superweak prediction holds for both charge asymmetries if the $\Delta S = \Delta Q$ rule is valid. From the K_{e3}^0 charge asymmetry measurements and a measurement[7] which yielded $F_e = (0.96 \pm 0.05)$ we obtain

$$F_\mu = (\delta_\mu/\delta_e)F_e = 1.79 \pm 0.46 \ .$$

If we assume that $\text{Im}(x_\mu) = 0$, as is consistent with the previous measurements[8] of x_μ and as is implied by T invariance in the muonic decay interaction, we obtain $\text{Re}(x_\mu) = 0.27 \pm 0.12$.

II. EXPERIMENTAL METHOD

A. Beam

The experiment was located at the end of the second channel of the external proton beam at the Lawrence Berkeley Laboratory's Bevatron. About 6×10^{11} protons per Bevatron pulse were received on a 12.7-cm copper target. The neutral beam (see Fig. 1) was defined by a series of tapered collimators to have a solid angle of approximately 0.2 msr about the production angle of 7°.

Charged particles were swept from the neutral beam by four sweeping magnets (Fig. 1). The first magnet was situated between the target and the first collimator.

B. Counters

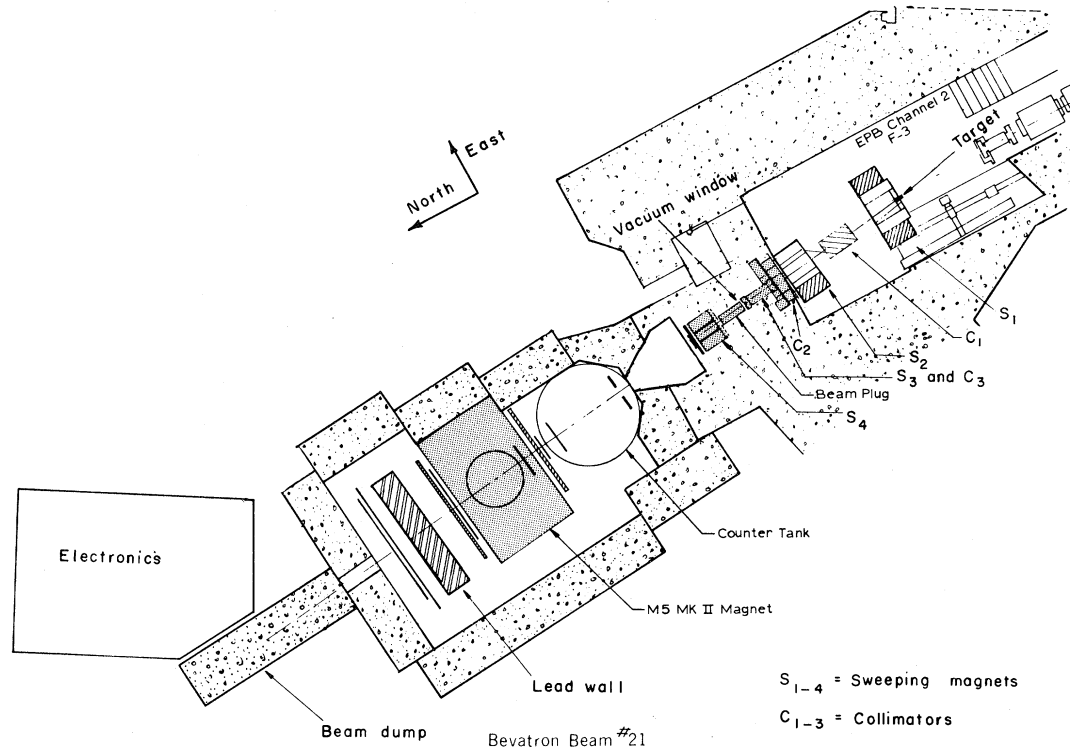The detection apparatus consisted of 154 scintillation counters monitored by a DEC PDP-9 com-

FIG. 1. Plan view of the Bevatron beam line.

puter. The important counter banks are labeled in Fig. 2. K_L^0 decays were identified by an up-down coincidence of the large trigger counters labeled P situated outside the neutral beam. The $K_{\mu 3}^0$ component of these decays was identified by separating muons from other particles by requiring penetration of a 61-cm-thick lead wall. Muons were required to traverse the lead wall and count in banks L and M. In addition, the muons traversed 5 cm of steel just downstream of the T counters and 5 cm of steel between banks L and M. Those muons reaching the N bank, not required for a $K_{\mu 3}^0$ signature, traversed a third 5-cm steel plate. The system was up-down symmetric. The muon could be up with the pion down or vice versa.

The system was designed to accept $K_{\mu 3}^0$ decays which had a vertex in the decay volume, produced a muon with sufficient momentum to penetrate the lead wall, but yet also produced both a muon and a pion with sufficient transverse momentum to get out of the beam (i.e., cross over the beamside edge of the appropriate P counter). In order to accept these muons the counter banks increased in size from the upstream end of the experiment to the downstream end (see Fig. 2). The expected muon track would contain P, S, R, T, L, M, and perhaps N counts. The pion could indicate its presence by a lone P count or, if it stayed close

to the beam it might produce counts further down-stream.

The charge-resolving magnet ($M5$) had circular pole faces with a diameter of 160 cm and a gap of 132 cm. The field pointed up or down. The $M5$ imparted a transverse momentum of about 500 MeV/c to particles passing through it. Since the maximum transverse momentum of a muon in $K_{\mu 3}^0$ decay is 216 MeV/c, negatively charged muons were given a complete angular separation from positively charged muons. One method of muon charge determination was to observe whether the position of the muon at the L hodoscope was east or west of the center line. In the absence of multiple scattering in the lead wall this method of charge determination would have been completely unambiguous. The charge was also determined by measuring the direction of the muon curvature in the $M5$. This determination was accomplished using the S, R, and T hodoscopes. The method used to bin the muon position in the S, R, and T banks is depicted in Fig. 3. For the purpose of binning, the L, M, and N banks formed one logical bank called W, also shown in Fig. 3.

The ratio of high-energy neutrons to long-lived K mesons in the neutral beam was large, about two hundred to one. Figure 4 shows the rough neutron and K_L^0 momentum spectra at the Beva-
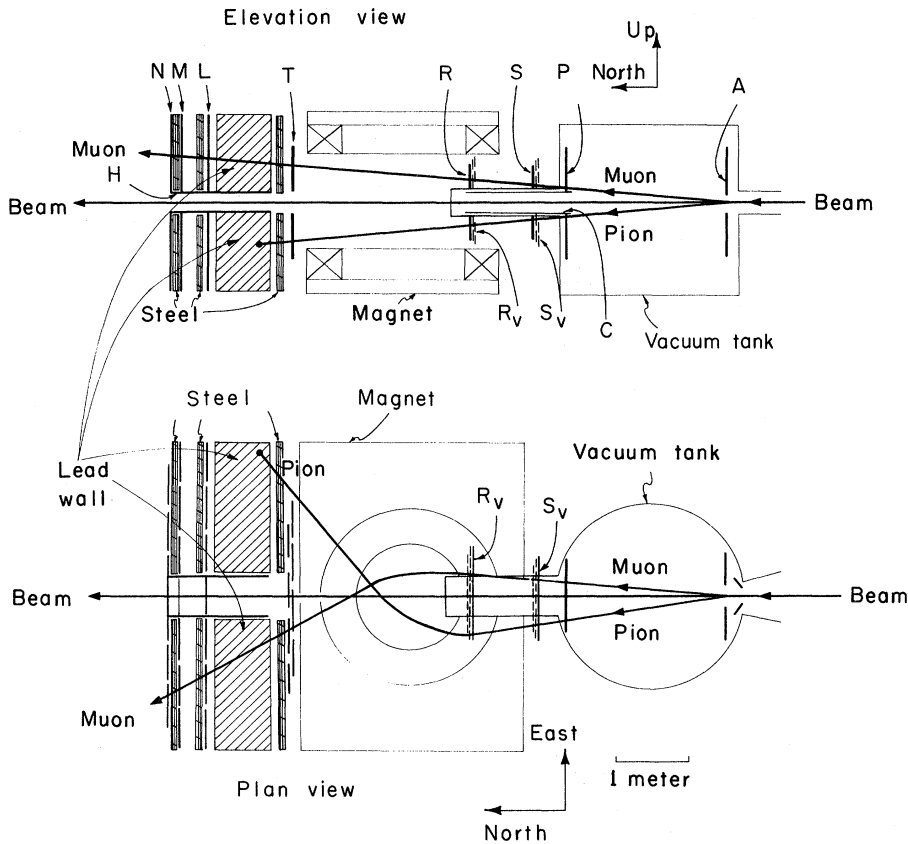
Elevation view

FIG. 2. Layout of the experimental apparatus.

tron. In order to avoid contamination of the K sample by neutron interactions, all mass was removed from the neutral beam in the decay volume. The geometrical details are illustrated in Fig. 5. The vertical beam profile is indicated showing both the umbra and the large penumbra which was a result of the necessity of collimating close to the target. The anti counter (A in Fig. 2) was actually a set of six counters which acted as a shield against charged particles coming from upstream. It was logically equivalent to a single large counter with a hole in it slightly bigger than the beam. The vertical separation of the upper and lower portions is indicated on Fig. 5 along with the positions of the P counters. An event was accepted only if counts were observed in both P counters but not in the anti counter. Thus, an event originating at a vertex must have originated downstream of the intersection of the two lines L_1 and L_2 defined by the edges of the A and P counters. In this manner, the decay volume was defined without putting any mass into the beam.

The entire decay volume was kept at vacuum (typically 10^{-5} atmosphere). The A, P, and C counters were inside the vacuum tank, and the beam passed into the vacuum through a thin win-

dow (0.025 cm aluminum) just downstream of the last sweeping magnet. In order to keep neutron interactions as far as possible from the P counters, the beam was brought out of the vacuum tank into a vacuum snout which extended well into the $M5$ (Fig. 2).
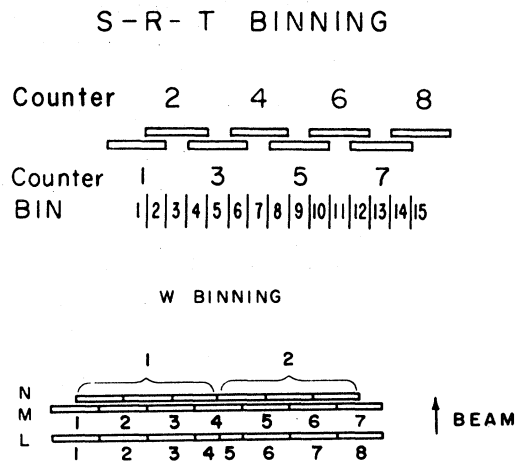
S – R – T BINNING

W BINNING

FIG. 3. S-R-T and W binning schemes.

The S_V and R_V counters shown on Fig. 2 provided vertical resolution. Their geometry is shown in Fig. 6(a). For events in which the pion reached the R bank, these counters were used in conjunction with the S and R counters to reconstruct the decay vertices.

Figure 7 shows the vertex distribution. Due to randoms and scattering in the vacuum tank wall on the pion side, the long tail extending upstream is expected, and because of pion interactions, the events in the tail are expected to have a charge asymmetry. However, the events upstream of -300 in. only change the charge asymmetry of the whole sample by 3×10^{-4}. Hence the vertex distribution supports the contention that the upstream acceptance is well understood.

There were two known flaws in the trigger system. First, neutrons in the halo around the beam could have interacted in the anticounter itself. If charged particles were produced by such a neutron interaction sufficiently close to the downstream anti-counter edge, the particles would not have registered in the counter. Hence, such a neutron-induced event would have been accepted by the A-P system if these charged particles also counted in both P's.

The second source of error in the above trigger system is that it does not take into account neutron backscatter. Specifically, halo neutrons could have interacted in the walls of the vacuum snout and sprayed low-energy particles backward into both P counters. In order to measure the number and charge asymmetry of such events, the horizontal walls of the snout were lined with counters. Counters also were placed below P_{up} and above P_{down} to detect interactions in the P's themselves. The geometry of these guard counters (labeled C)

is presented in Fig. 6(b). Note that for a neutron interaction to have backscattered from the snout into both P's, both an upper C and a lower C must have counted. This was true even if the interaction occurred in a C counter.

A hole was made in the lead wall to allow the neutral beam to pass through. Unfortunately, this hole also opened a path by which pions could penetrate the lead wall. In order to eliminate these pions, the hole was lined with a steel beam conduit with walls 7.5 cm thick on the sides and 10 cm thick on top and bottom. The conduit was lined in turn with counters [labeled H, Fig. 6(b)] to detect particles passing through the conduit.

C. Electronics

Because the electronics system has been described elsewhere,[9] only an abbreviated description will be presented here. An on-line, interactive, counter control system was designed and built using a Digital Equipment Corporation PDP-9 computer, a Tektronix 611 CRT, and unique data-acquisition electronics. The system was capable of asynchronous and programmable electronic verification of the discriminator and coincidence circuits for each counter.
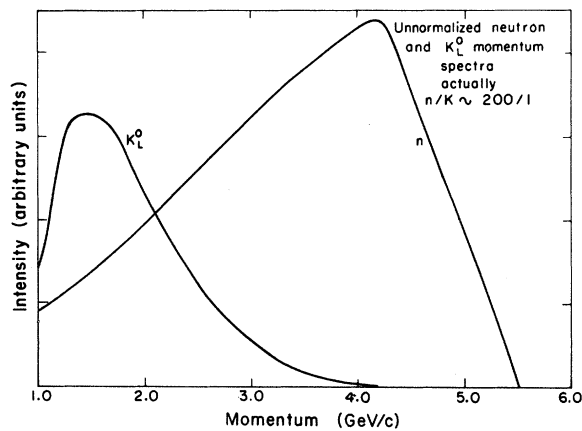

FIG. 4. Neutron and K_L^0 momentum spectra (unnormalized). The actual n/K ratio was about 200/1. Neutron spectrum from Ref. 15, and K_L^0 spectrum from Ref. 11.
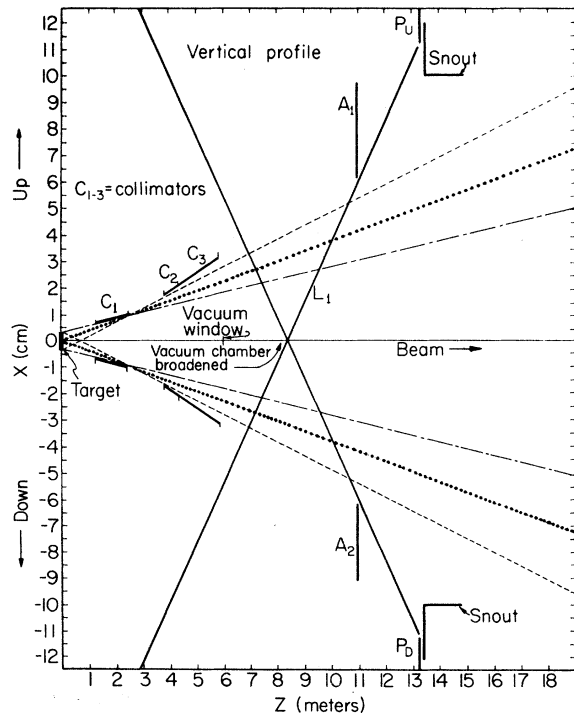

FIG. 5. Geometrical detail of definition of the decay volume by the A and P counters. Vertical scale is greatly expanded.

After threshold discrimination by a specially designed LBL discriminator, a typical photomultiplier anode signal produced three outputs. One output was used in the formation of a pulse called the *prompt strobe* which signified that the event under consideration had passed the acceptance criteria on the counter banks upstream of the lead wall. Counter information was stored only when such a strobe was generated. A second pulse for each counter was sent into a coincidence circuit
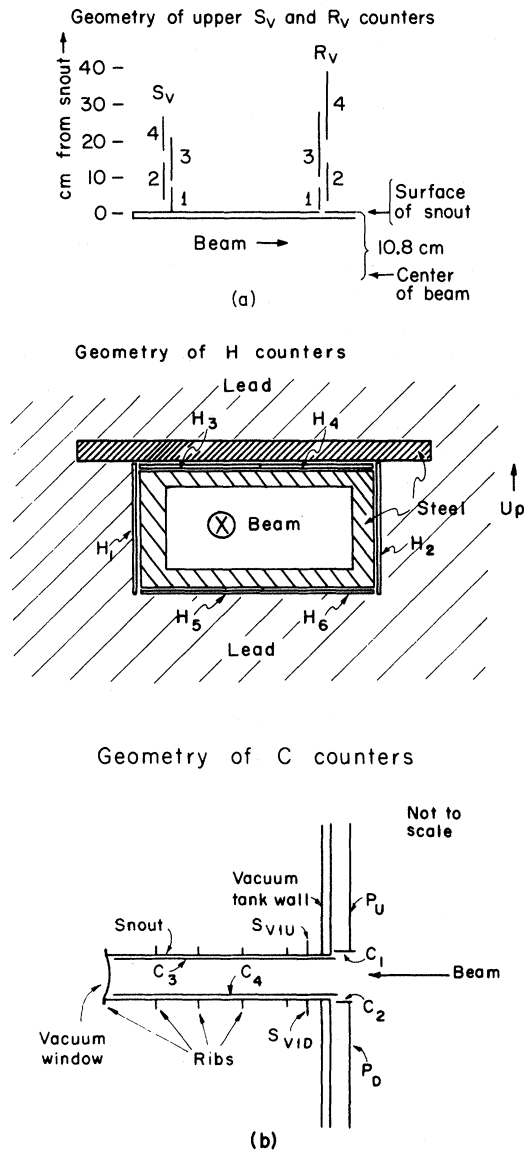
versus the prompt strobe. The resulting bit of information, whether or not the counter in question was on in time-correlation with the prompt strobe, was stored for the counter. A *delayed strobe* pulse was also generated precisely one Bevatron revolution (403 nsec) after the prompt strobe. This delayed strobe inquired if each counter was on in random time correlation with the prompt strobe. The reason for waiting one Bevatron revolution was to ensure that both time slots sampled the same beam structure.

The LBL discriminators, used primarily because of their low cost, had one serious drawback, a deadtime of about 20 nsec after any output pulse. In order to overcome this deadtime, the coincidence circuit resolving time was increased, so that if the pulse from a genuine event were "lost" due to deadtime, the coincidence circuit would respond instead to the spurious pulse which had produced the deadtime. The coincidence resolving time under these conditions was very long (60 nsec), about three times longer than would otherwise have been required.

The C, H, A, and P counters were not attached to LBL discriminators, but instead to commercial Chronetics discriminators run in a deadtimeless mode; subsequent to discrimination, their respective logical bits were treated electronically the same as the other counters.

Only the A, P, and S counters were involved in the strobe logic, generated by a set of Chronetics

Geometry of upper S_V and R_V counters

(a)

Geometry of H counters

Geometry of C counters

(b)

FIG. 6. (a) Vertical resolution counter layout (S_V and R_V counters). Note that S_{V1} and R_{V1} are in contact with the snout extending downstream of the main vacuum chamber. (b) Geometrical layout of the C, S_{V1}, and H counters.
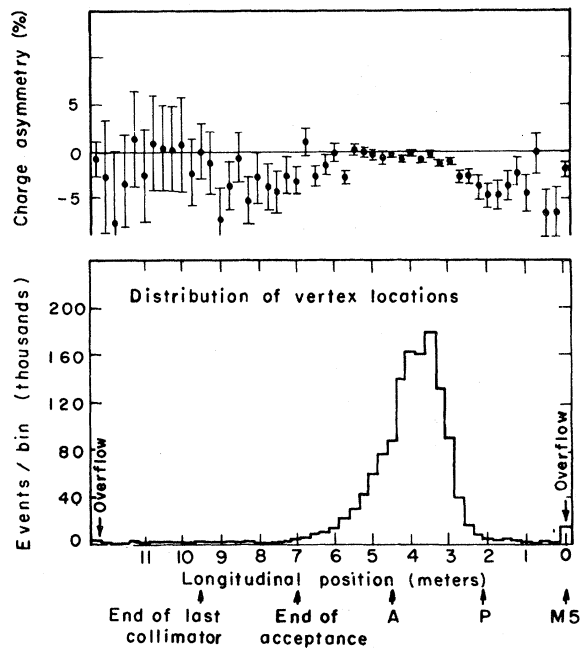

FIG. 7. Distribution of vertex locations, and charge asymmetry per vertex bin.

coincidence circuits. One additional criterion was imposed before an event was recorded by the computer. Using a matrix of coincidence circuits, the L and M counter bits were electronically analyzed, and the event was accepted only if there was a prompt time (or delayed time) coincidence between at least one L and one M counter. The event was then read out to the PDP-9 computer, to be recorded on magnetic tape at the end of the Bevatron pulse cycle.

Let

$\overline{A}$ = lack of an A count,

$[P]$ = P counter delayed 403 nsec,

U, D = up, down,

$P_U P_D$ = coincidence between P_U and P_D,

S_D = "OR" of 13 S-down counters.

Then if

$$V_D \equiv \overline{A} P_U P_D \text{ OR } [\overline{A} P_U] P_D$$

and

$$V_U \equiv \overline{A} P_U P_D \text{ OR } [\overline{A} P_D] P_U ,$$

the prompt strobe was

Prompt strobe $\equiv \overline{A} V_D S_D$ OR $\overline{A} V_U S_U$.

Thus the system was triggered not only on prompt events but also on the two random configurations which were most important: a muon track with a random pion P count (delayed P event) and an $\overline{A} VS$ with a random LM signal (delayed W event).

The system also contained six analog-to-digital converters, which were used to do pulse-area analysis (PAA) and time-to-pulse-height analysis (TPH) of the various counters.

III. DATA ANALYSIS

A. General Analysis

The data from the experiment are stored on approximately 200 reels of magnetic tape; the analysis was done on the Lawrence Berkeley Laboratory's CDC 6600B computer.

Approximately 24 million events were recorded on tape during the data-taking phase of the experiment. About 9 million of these events satisfied a $K^0_{\mu 3}$ signature criterion. Most of the unacceptable triggers which failed the signature tests were random triggers. The dominant type was of the kind in which the R and T banks (not required in the trigger) were missing.

The $K^0_{\mu 3}$ signature required in the analysis was much more restrictive than the electronic trigger requirement. The signature requirements for prompt and delayed P events were as follows:

prompt: $\overline{A} P_D P_U S_U R_U T_U W_U$ OR $\overline{A} P_U P_D S_D R_D T_D W_D$,

delayed P: $\overline{A} P_U S_U R_U T_U W_U$ OR $\overline{A} P_D S_D R_D T_D W_D$.

Here $\overline{A}$ signifies a bit which was sent to the computer indicating whether or not the anti counter was on. A bit was also sent to the computer indicating whether the information was associated with a prompt or delayed P count.

For a delayed W event, the OR of prompt and delayed bits was formed for each counter before performing the same signature test as carried out on prompt events. If a delayed T count was associated with a delayed W, this information was preserved.

The analysis was performed in two stages. The first-pass analysis program calculated and binned for each event the following four quantities char-
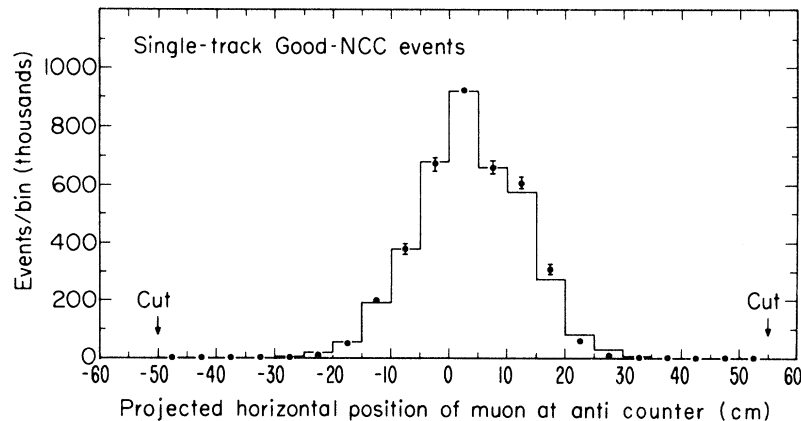

FIG. 8. Single-track good-NCC events. Number of events vs projected horizontal position of muon track, if extended back to the anti counter position. The Monte Carlo calculation is also shown, normalized to the peak.
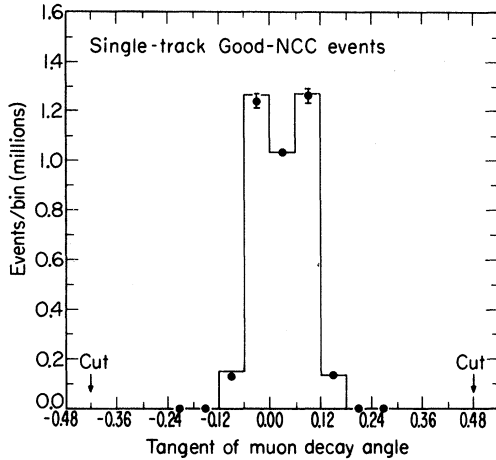
FIG. 9. Single-track good-NCC events. Number of events vs tangent of muon laboratory decay angle. The Monte Carlo calculation is also shown, normalized to the central bin.

acterizing horizontal projection of the muon trajectory: decay angle, projected position at the anticounter, bend angle in the $M5$, and scattering angle in the lead wall. The position of a muon at a given bank was taken to be the center of its bin in that bank.

The second-pass analysis program then made cuts on each of these four quantities. Events which did not possess a muon trajectory with acceptable values of all four of them were excluded from further analysis. The first-pass analysis and a Monte Carlo calculation were used to determine the points at which to make the cuts. Figures 8–11 show the points at which the cuts were made. The cuts appear to be quite liberal, as they must be; the result of the experiment is insensitive to the positions of the cuts. After the neutron cut (also discussed below) the second-pass cuts only changed the charge asymmetry by −0.15%.
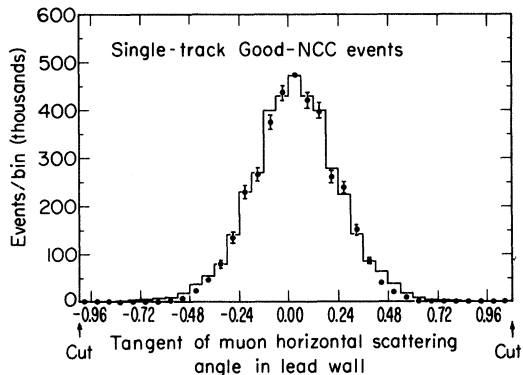

FIG. 10. Single-track good-NCC events. Number of events vs tangent of muon horizontal scattering angle in lead wall. The Monte Carlo calculation is also shown, normalized to the peak.

B. Monte Carlo Program

The Monte Carlo program for this experiment was written in order to perform several important calculations and in general to test and enhance our understanding of the experiment. Approximately five thousand $K_{\mu3}^0$ events were generated in the K-meson rest frame in accordance with the $V - A$ theory as given by Okun'.[10] The K_L^0 mesons were given a momentum distributior in accordance with a recent measurement at the Bevatron,[11] done at a K_L^0 production angle of 3.7°. This spectrum was extrapolated to our production angle of 7° using a well-known prescription.[12] Multiple scattering was calculated in the Gaussian approximation. Energy loss was computed using a linear approximation to the muon energy-loss tables. Energy-loss straggling was calculated according to the theory of Symon as given by Rossi.[13]

In Figs. 8–11 the Monte Carlo predictions for various distributions are compared with the data. Statistical error bars are shown if they are bigger than the corresponding points. Agreement is good between the predicted and actual distributions in all cases. (The slight broadening of the actual peaks in the bend-angle and scattering-angle distributions is thought to be due to 1-bin-shift knockons, to be discussed below.) The Monte Carlo predictions are shown in Fig. 12 for the muon and pion momentum spectra occurring in accepted events.

C. Mass Extrapolations

Three effects (pion absorption in the P counters, neutron interactions in the anti counter, and neutron interactions in the residual air in the decay
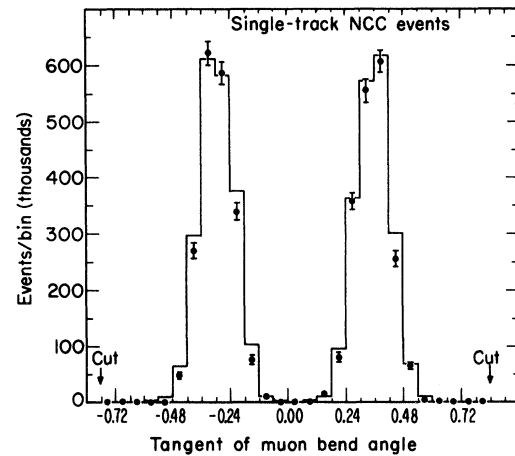

FIG. 11. Single-track NCC events. Number of events vs tangent of muon bend angle in the magnet. The Monte Carlo calculation is also shown, normalized to the peaks (sum of two bins).
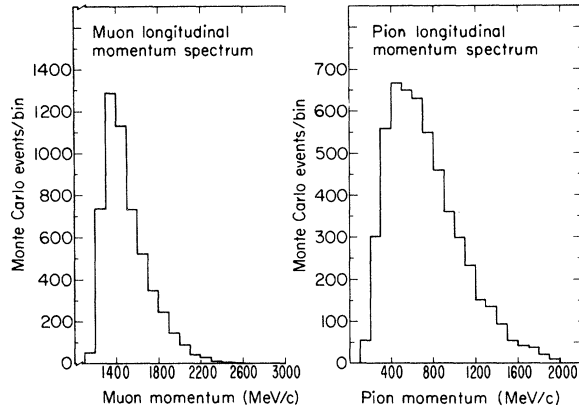
FIG. 12. Monte Carlo predictions for the pion and muon longitudinal-momentum spectra.

volume) are treated through the use of linear mass extrapolations. The procedure is to add mass in various regions of the apparatus in order to extrapolate the charge asymmetry to the result which would be obtained by an ideal zero-mass detector. In all extrapolations the added material was identical to that used in the detector. The zero-mass intercept was found by doing a minimum-χ^2 fit of the measured points to a straight line.

IV. CORRECTIONS

A. Introduction

Table I contains a summary of all of the various corrections. Two of the most important are due to the "neutron cut" (described in detail below, in which certain high momentum trajectories are excluded) and the presence of knock-on electrons, which produce ambiguous events. Each of these two has been assigned a systematic error of $\pm 5 \times 10^{-4}$. The range difference between μ^+ and μ^- is responsible for a third large correction with a systematic error of $\pm 7 \times 10^{-4}$. The correction for the dilution of the charge asymmetry due to pion decay in flight has a similar systematic error when listed as an additive correction.

A correction to the charge asymmetry was considered negligible if it was less than 10^{-4} in magnitude and error (one standard deviation). The term "good events" will be defined below. These events made up the relatively uncontaminated portion of the data remaining after a cut had been employed to free the data of neutron interactions. The term "uncorrected good events" refers to these events after the neutron cut had been made but before any other corrections had been applied (including the knock-on correction which was associated with the neutron cut).

In all histograms, event lists, and calculations, the delayed W and delayed P random-trigger events have been subtracted (bin by bin where applicable) unless otherwise noted.

B. Reversal of the Magnetic Field

Frequent reversal of the charge-resolving magnetic field is the cornerstone of the experimental technique required to do this experiment. We de-

TABLE I. Determination of the charge asymmetry (all numbers in units of 10^{-4}). The errors under "total" are the results of combining the numbers in the individual columns in quadrature.

| | | Errors | |
	Value	Statistical	Systematic
After neutron cut	$\delta = +51.6$	± 4.9	± 5.0
Knock-ons	$\Delta\delta = -45.4$		± 5.1
Anti mass	$\Delta\delta = +3.8$	± 1.2	± 1.2
Randoms	$\Delta\delta$ included		± 2.0
P mass	$\Delta\delta = +0.9$	± 3.6	
$\pi^\pm$ penetration	$\Delta\delta = $ none		
Decay in flight asymmetry	$\Delta\delta = +5.7$		± 1.0
dilution	$\Delta\delta = +8.2$		± 7.1
$\mu^\pm$ range difference	$\Delta\delta = +31.0$		± 7.0
$\mu^\pm$ end of range	$\Delta\delta = +3.9$		± 1.5
Total	$\delta = +59.7$	± 6.2	± 12.6

fine:

$N \equiv$ total number of K^0_L which decayed to $\pi\mu\nu$ downstream of our last collimator during the experiment,

$\eta_{R,L} \equiv$ efficiency for detecting these $K^0_{\mu 3}$ events if the muon bent right (or left),

$N_\pm \equiv$ number of $K^0_{\mu 3}$ in N having a $\mu^\pm$,

$n_\pm \equiv$ number of $K^0_{\mu 3}$ detected having a $\mu^\pm$.

The true charge asymmetry in $K^0_{\mu 3}$ decays (within the statistical error on N) is

$$\delta = \frac{N_+ - N_-}{N_+ + N_-} \pm \frac{1}{\sqrt{N}} \ .$$

We define the efficiency asymmetry to be

$$a = \frac{\eta_R - \eta_L}{\eta_R + \eta_L} \ .$$

If ↑ and ↓ denote events taken with the field up and down, respectively, then we have $N^\uparrow + N^\downarrow = N$, and

$$\delta^\uparrow = \frac{N^\uparrow_+ - N^\uparrow_-}{N^\uparrow_+ + N^\uparrow_-} \ ,$$

$$\delta^\downarrow = \frac{N^\downarrow_+ - N^\downarrow_-}{N^\downarrow_+ + N^\downarrow_-} \ .$$

The geometric bias[14] is defined to be

$$\Lambda \equiv \tfrac{1}{2}\left(\frac{n^\uparrow_+ - n^\uparrow_-}{n^\uparrow_+ + n^\uparrow_-} - \frac{n^\downarrow_+ - n^\downarrow_-}{n^\downarrow_+ + n^\downarrow_-}\right)$$

$$= \tfrac{1}{2}\left(\frac{\delta^\uparrow + a^\uparrow}{1 + a^\uparrow \delta^\uparrow} - \frac{\delta^\downarrow - a^\downarrow}{1 - a^\downarrow \delta^\downarrow}\right) \ ,$$

where we have included the possibility that the efficiencies might depend on the sign of the magnetic field. In this experiment, the δ's and a's all are $< 10^{-2}$. So to an accuracy of 10^{-4} of Λ,

$$\Lambda = \tfrac{1}{2}(\delta^\uparrow - \delta^\downarrow) + \tfrac{1}{2}(a^\uparrow + a^\downarrow)$$

$$= \tfrac{1}{2}(a^\uparrow + a^\downarrow)$$

$$= a.$$

The geometric bias is equal to the average asymmetry of the efficiencies. The expression which was used to define the measured charge asymmetry is as follows:

$$\delta_{\text{measured}} = \frac{n^\uparrow_+ - n^\uparrow_- + n^\downarrow_+ - n^\downarrow_-}{n^\uparrow_+ + n^\uparrow_- + n^\downarrow_+ + n^\downarrow_-} \ .$$

To an accuracy of 10^{-4} of δ_{measured} ,

$$\delta_{\text{measured}} = \delta + \tfrac{1}{2}(a^\uparrow - a^\downarrow) + \Lambda\alpha,$$

where

$$\alpha \equiv \frac{N^\uparrow - N^\downarrow}{N^\uparrow + N^\downarrow} \ .$$

Here α is zero if an equal number of events are taken with the field up and down. For this experiment, the last term in δ_{measured} is negligible (1.0×10^{-6}). However, from the expression for the measured charge asymmetry it can be seen that it is crucial that the efficiencies must not depend on the sign of the magnetic field; a difference in the efficiency asymmetries with the field up and down enters directly into the measured charge asymmetry. There are two ways that the efficiencies might depend on the sign of the field: via the counting efficiency of the detectors, and via the geometrical efficiency of the volume occupied by the detectors. These two possibilities will be considered in turn.

The reason for reversing the magnetic field frequently is to cancel out the effect of a possible slow, long-term variation of the efficiency asymmetry. The magnetic field was reversed approximately every 10 000 events for a total of about 600 reversals during the data-taking phase of the experiment.

C. Counting Efficiency

A major advantage of having performed this experiment with counters rather than spark chambers is that the counting efficiency was measured very accurately. It can be demonstrated that the efficiency asymmetry did not change with the magnetic field reversals to an accuracy of one part in 10^4.

All counters in the A, P, S, R, T, L, M, N, and H banks were tested in a π^- auxiliary beam of 2.8 GeV/c before their use in the main experiment. Each counter had its high voltage set at a level such that the inefficiency (measured by comparing 4-fold to 5-fold coincidences) at the worst spot on the counter was less than 10^{-4} with the output pulse attenuated by a safety factor of 2 (factor of 1.25 for the W counters). During the data-taking phase of the experiment the counter pulse heights were periodically monitored with an oscilloscope. The pulse height of any counter required in the $K^0_{\mu 3}$ signature was never observed to have sunk so low that its inefficiency became greater than 10^{-4}, considering the above safety factors.

Pulse-area analyses were also performed for every counter (except the anti counters) required in the $K^0_{\mu 3}$ signature using muons from the prompt events. The peak position never shifted beyond the PAA measurement error of ±7% with the reversal of the magnetic field, which is another confirmation that the efficiency of each counter was constant under field reversal to one part in 10^4. This implies that the efficiency asymmetry was also constant to one part in 10^4. All counting rates

were also checked approximately every four hours while taking data, and no counter required in the $K^0_{\mu 3}$ signature ever failed.

D. Geometrical Efficiency

One way that the geometrical efficiency of the counters could have changed with field reversal is that the field may have indeed not reversed completely. Suppose that under reversal, the field actually changed from $(-B)$ to $(+B + \Delta B)$. In this case, more muons would have been bent outside the region subtended by the T bank, resulting in a loss of efficiency with the field up. This effect alone would still not have caused a change in the measured charge asymmetry since η_R and η_L would have changed by equal amounts. Only a change in the *efficiency asymmetry* would have affected our measurement. However, such a nonreversal of the field could have combined with misalignments or the horizontal asymmetry of the beam to produce a change in the efficiency asymmetry. The experiment was designed in such a way that the major $K^0_{\mu 3}$ acceptance cuts were made before the magnetic field, so that the efficiency asymmetry would be insensitive to field nonreversal. The field was monitored by three coils which were flipped pneumatically approximately once every four hours. Using these coils, it was determined that the total field integral reversed to an accuracy of $\pm 0.2\%$.

In order to study the effects of a possible nonreversal of the total field integral a series of runs was taken with the magnet current set 2% below its normal value. For a 2% decrease in the current, the measured change in the efficiency asymmetry was $\Delta a = (-2.4 \pm 3.0) \times 10^{-3}$. As the field is known to reverse to at least $\pm 0.2\%$, the maximum effect on the charge asymmetry was

$$\Delta \delta_{\text{measured}} = \tfrac{1}{2} \Delta a$$
$$= (-1.2 \pm 1.5) \times 10^{-4}.$$

However, because any possible field nonreversal was probably due to the accuracy with which the current could be set, and was therefore random, no correction will be made.

E. Charge Determination

Neither method of charge determination used in this experiment was without fault. The L counters could provide the wrong sign for a small fraction of the muons, due to multiple Coulomb scattering in the lead wall. The sign could also be ambiguous if the W-bin criteria were satisfied on both west and east sides of the L bank. The S-R-T determination was often ambiguous if an extra S, R, or T counter was on, or if the track under considera-

tion had high enough momentum so that it looked essentially straight in the apparatus. The term "track" will be used to describe a combination of S, R, T, and W bins which represents a trajectory. If an event had more than one muon track, the S-R-T charge determination was unambiguous only if all tracks had the same sign of curvature. Table II shows the number of events possessing each possible type of charge determination. The results are presented for the data sample labeled "good-NCC" (ALL events excluding CC events) which will be used to calculate the $K^0_{\mu 3}$ charge asymmetry.

The charge resolution is quite good. As a fraction of the total number of events

4×10^{-4} fail S-R-T determination ,

4×10^{-4} fail L determination ,

3×10^{-5} fail both ,

3×10^{-3} have disagreement between the two methods.

The S-R-T method is chosen to determine the muon charge when possible. Where the S-R-T method fails, the L method is used. If the failure in the S-R-T method is uncorrelated with a wrong decision in the L method, then the wrong charge is chosen for only 1×10^{-6} of the events.

The reason that the charge resolution is so good for the above sample is that many of the problems have been excluded in the bend angle (neutron) cut to be discussed below. The S-R-T method fails mainly for events with a small bend angle for two reasons: it cannot resolve a straight track, and an event with two tracks of opposite charges is likely to have one track with a small bend angle (where the charge of the trajectory changes). As explained below, the track with the smallest bend angle is chosen to represent a multiple track event.

In the above data sample, the double penetration events which possess muon tracks both up and

TABLE II. Types of charge determination for events with bend-angle bin ≥ 0.24, excluding C-coincidence events. The curvature and position methods of charge determination can each find the muon charge to be $+$, $-$, or ambiguous.

Position method	Curvature method		
	$-$	ambiguous	$+$
$-$	2 055 651	854	7169
ambiguous	624	143	706
$+$	7032	744	2 076 950
		Total $= 4\,149\,873$	

down have been omitted. For these events, comprising $(0.22 \pm 0.01)\%$ of the data, the muon cannot be identified. A Monte Carlo calculation predicts that $(0.21 \pm 0.03)\%$ of the data are double penetration events due to pion decay in flight from $K_{\mu 3}^0$. Hence it is believed that these events are understood.

F. Neutron Interactions

Figure 4 shows the neutron and K_L^0 momentum spectra.[15] The neutron spectrum is peaked at very high momentum and thus unfortunately can produce very high-momentum secondaries. One type of neutron interaction which could have been accepted involves low-energy spray to trigger the P counters and a fast hadron with very high momentum to penetrate the lead wall. Another type of neutron interaction (not requiring that a hadron penetrate the wall) would involve decay in flight of a fast pion.

Some data were taken with the anticounter requirement removed from the trigger. It was found that for events satisfying a $K_{\mu 3}^0$ signature requirement (with the exception of the anti-counter requirement), the ratio of the number of events with anti counter on to anti counter off was (1.1). The charge asymmetry of the events with the anti counter on was $(0.4 \pm 0.9)\%$. Thus the maximum contribution to the measured charge asymmetry due to anti counter inefficiency is 4×10^{-7} using an inefficiency of 10^{-4}. Hence we believe that the anti counter was effective and therefore neutron interactions could have triggered our system from only two places: the snout area and the anti counter itself. These two possibilities will be discussed separately below.

1. Neutron Cut

There were two means of detecting neutron interactions in the snout [Fig. 6(b)]: the C counter updown coincidence, and the S_V counter, labeled S_{V1}, nearest the beam on the muon side. Neither means could be used as an absolute veto to exclude neutron events. The S_{V1} detected the events coming from the most likely area of origin, the upstream portion of the snout and the vacuum tank wall near the beam. The C counter coincidence could not be used as an absolute veto mainly because pions from $K_{\mu 3}^0$ might have interacted asymmetrically in the snout before triggering the coincidence.

Because there was no absolute neutron veto, the philosophy was adopted of studying the data in the hope that a portion of it was free of neutrons and hence insensitive to the state of the C coincidence and S_{V1}. In order to aid in this study, the following

abbreviations will be adopted:

  ALL = all events (surviving second-pass cuts),
  CC = events with C coincidence on,
  NCC = ALL events excluding CC events,
  CCSV = events with C coincidence and S_{V1} on,
  NCCSV = ALL events excluding CCSV events.

In the following discussion a series of plots will be presented containing as the abscissa the magnitude of the tangent of the muon bend angle in the $M5$ magnet. This quantity will generally be referred to simply as the "bend angle." The bin size used for the bend angle is 0.06. From the geometry of the counters, the calculated bend angle resolution is ± 0.12. Thus it is possible for an event to appear as much as two bend-angle bins from its true location.

To see the effect of the C-counter coincidence on the data, Fig. 13 shows the distributions of the number of events and charge asymmetry vs bend angle for the NCC and CC *single-track* events. *Neutron contamination is evident.* There is a very large charge asymmetry in the high momentum bins, where very few muons from $K_{\mu 3}^0$ are expected. A strong correlation between the charge asymmetric events and the C coincidence is seen, indicating that many of these events originated in the snout downstream of the vacuum tank. The
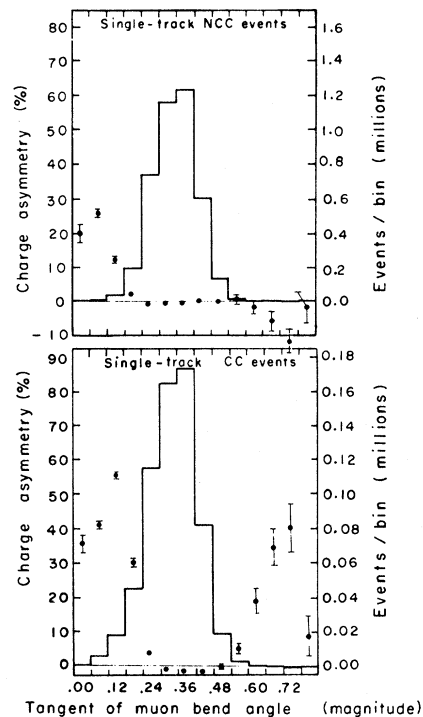

FIG. 13. Single-track NCC and CC events: Number of events and charge asymmetry vs bend angle. Note that the vertical scales (events/bin) differ in the two parts of the figure.

large charge asymmetry in the high-momentum NCC events is mainly due to neutron interactions in the anti counter. Apparently, whether the event was made in the anti counter or the snout the culprit was the same: the type of neutron interaction in which a hadron penetrated the lead wall. These events appear to have left relatively uncontaminated much of the region where the real muons are expected (bins 0.24–0.48) as in Fig. 11.

The low-momentum events also show a charge asymmetry which is correlated with the C coincidence. The nature of these events is somewhat puzzling because the minimum muon momentum penetrating to the M bank is 1075 MeV/c (bend-angle bin 0.48). One possibility is that they are neutron induced events, where the neutron penetrates the lead wall and converts to form a W bin. The S-R-T requirement could then be satisfied by a pion, associated with the neutron, which does not penetrate the wall but happens to point to the neutron's W. In that case one would be measuring the charge of the pion. These events will be included in the good event sample and the uncertainties associated with them will be incorporated into the systematic error of the neutron cut. However, these events represent no problem. There are so few of them that the effect on the charge asymmetry is less than 10^{-4}.

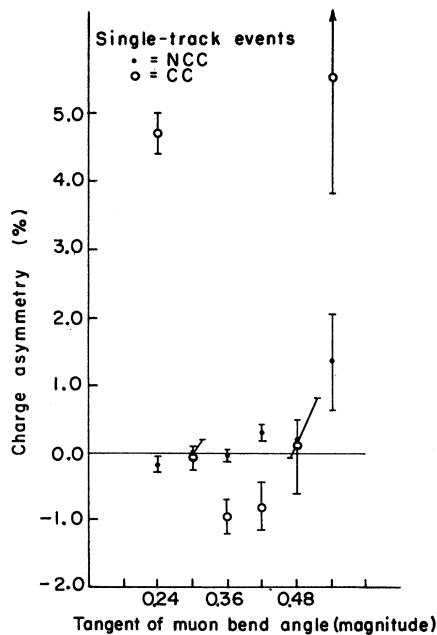Figure 14 is an expanded view of the charge asymmetries under the muon peak. There are

systematic differences between the NCC and CC events throughout the plot. In bins 0.24 and 0.54 the differences are apparently due to the high- and low-momentum background events just discussed. In bins 0.36 and 0.42, however, the CC events have a negative charge asymmetry. There are two likely causes for this asymmetry: neutron interactions where the particle penetrating the lead wall is a muon from pion decay in flight, or asymmetric interactions of pions from $K^0_{\mu 3}$ before triggering the C coincidence. The first type of event should not be included in the charge asymmetry measurement while the second type should. Hence, the net effect of these events on the charge asymmetry represents a systematic error. The most likely explanation is that these events are produced by neutrons since the neutron interactions in the anti counter have a negative charge asymmetry in this region (as discussed below).

The size of the systematic error introduced by neutron interactions is studied in Fig. 15. Here the asymmetries of the NCC, ALL, and NCCSV events are plotted in order to study the effect of the CC events on the charge asymmetry of each bin. The statistical errors of the NCC points have been indicated. With the sole exception of bin 0.24, the difference between the ALL and NCC asymmetries is about equal to or less than the NCC statistical error. The NCCSV curve, however, shows agreement with the NCC curve for all

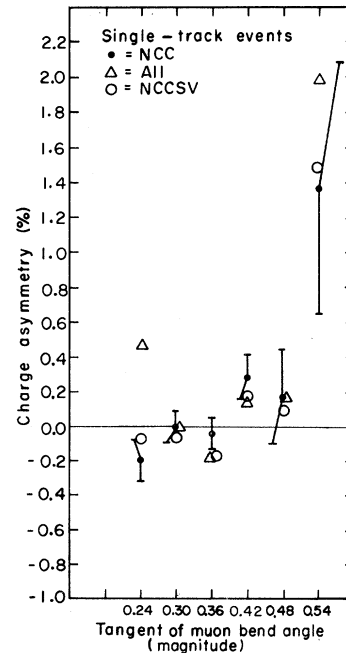FIG. 14. Single-track NCC and CC events: Comparison of charge asymmetries (expanded view).

FIG. 15. Single-track NCC, NCCSV, and ALL events: Comparison of charge asymmetries (expanded view).

bins including bin 0.24. Hence the discrepancy in bin 0.24 is due entirely to CCSV events, which have been labeled as neutron candidates by *both* means of identification. If the CCSV events from bin 0.24 are excluded, apparently the systematic error in excluding neutrons can be reduced to about the same size as the over-all statistical error. Thus we define the term "good event":

good events = NCCSV events with bend angle
bin $\geqslant 0.24$

+ CCSV events with bend angle
bin $\geqslant 0.30$.

There are 4 380 674 good, single-track events in the main data sample. The exclusion of all events with bend angle bin $\leqslant 0.18$, and CCSV events in bin 0.24 will be termed the "neutron cut."

Using Fig. 16, the neutron cut can be examined from an integral point of view. Here the NCC, NCCSV, and ALL charge asymmetries have been plotted for all bend angles greater than or equal to a given value. For the total sample, the CCSV events have a large effect on the charge asymmetry (about 0.6%). However, after bin 0.18 has been cut away, this effect has been reduced to about 0.1% (two NCC standard deviations). The effect then remains at about one NCC standard deviation across the muon peak.

The neutron cut includes 92% of the single-track data in the good event sample. Note that the charge asymmetry of good-NCC single-track events (bend angle bin $\geqslant 0.24$) differs from the good event single-track charge asymmetry by only 2×10^{-4}:

δ(good-ALL, single-track) = $(-2.2 \pm 4.8) \times 10^{-4}$,

δ(good-NCC, single-track) = $(-0.1 \pm 5.1) \times 10^{-4}$.
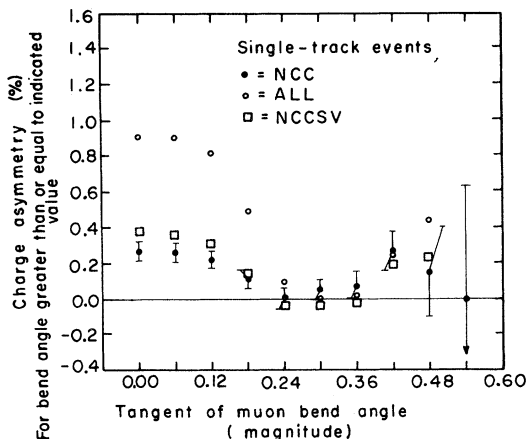

FIG. 16. Single-track NCC, NCCSV, and ALL events: Integrated charge asymmetry for all events in all bend angle bins $\geq$ indicated abscissa.

The independence of the charge asymmetry from the state of the C coincidence (as is apparent from these numbers and from Fig. 16) is the reason for believing that the "neutron cut" does indeed exclude the effects of neutrons. The strong correlation between neutron-induced events and the state of the C coincidence is proved by the high-momentum bins of Fig. 16. The effectiveness of the neutron cut is obviously due to the fact that most of the neutron interactions which trigger the system are associated with hadrons penetrating the lead wall; such penetration apparently requires a much higher momentum than is required for a muon penetration.

"Multiple-track events" are those with more than one track on the muon side of the apparatus. In most cases, these events had only one extra bin firing in one of the S, R, T, or W banks with only one bin firing in the other three, producing an ambiguity. Multiple-track events constitute 10.8% of the data which pass the second pass cuts. Because of the need for a neutron cut, these events are a serious problem. If such an event has an extra S, R, or T counter on, there is an ambiguity in its assignment to a bend-angle bin. In order to be sure to exclude the high-momentum neutron-induced events, when such an ambiguity arises, *the track with the smallest bend angle is chosen to represent the event*. This procedure, though necessary, causes serious problems in the analysis of events with knock-on electrons.

Consider a μ^- which makes a knock-on in the R counters. The electron will spiral around in the magnetic field and, if it has sufficient energy, it may count in an R bin separate from that of the muon. Since the knock-on has the same charge as the μ^-, it will always spiral in the same direction as the μ^- bends. Hence, the track including the knock-on R count will always have a higher momentum than the real μ^- track (unless the knock-on travels so far that its track has the curvature of a μ^+). By the same reasoning, a μ^+ can only produce a knock-on track of lower momentum. Hence, due to the above analysis procedure, knock-ons will shift μ^- tracks to smaller bend angles but will leave μ^+ tracks in their proper bins. Then the neutron cut, when applied to multiple track events, will preferentially exclude μ^-.

Aside from the large effects of knock-ons, the multiple-track data are qualitatively the same as the single-track data.[3] Figure 17 presents the integral curves for all events (single and multiple track) and corresponds to Fig. 16. The uncorrected charge asymmetries for good events and good-NCC events are as follows:

$\delta_{\text{good}} = (5.03 \pm 0.46) \times 10^{-3}$,

$\delta_{\text{good-NCC}} = (5.16 \pm 0.49) \times 10^{-3}$.

The two numbers are essentially identical. The second one is the best value for the charge asymmetry before other corrections. The above errors are statistical only. In accord with the previous discussion an additional systematic error of 5.0 $\times 10^{-4}$ (equal to the statistical error) is applied to take into account the inability to exclude the effects of neutrons.

About 4.4% of the events are multiple-track due to randoms. From the analysis to be described below it is shown that an additional 4.7% are multiple-track from knock-on events. Thus these two sources account for most (and perhaps all) of the 10.8% of the data with multiple tracks.

Since it has been shown that the good events and the good-NCC events are equivalent, only the good-NCC events will be considered in the discussion of the remaining corrections.

2. Residual Air in the Decay Volume

In order to perform the residual air mass extrapolation, a small amount of data was taken with the vacuum tank at atmospheric pressure. A total of 3180 events was accumulated with bend-angle bin ≥ 0.24, with a charge asymmetry of -3.5%. As the ratio of mass added to initial mass was about 10^5, the correction is negligible.

3. Anti-Counter Mass Extrapolation

Figure 18 shows the charge asymmetry as a function of anti-counter effective thickness. The high-mass points of this plot were taken with scin-
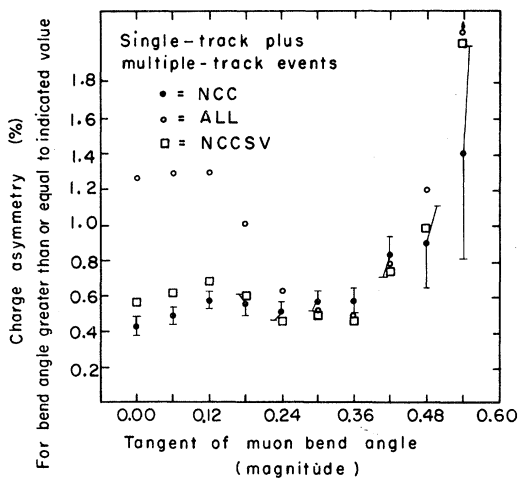
tillator placed just downstream of each of the six separate anti counters, so as to increase the inactive volume of each counter in which neutrons could generate background events. The fractional inactive length of each counter was taken to be the ratio of the electronic discrimination level to minimum-ionizing pulse height. However, more than one charged particle must have been created by any relevant neutron interaction, in order to trigger the P's. Since neutron interactions often have high multiplicity, and the secondaries may have high ionization losses, the average multiplicity is taken to be 3^{+3}_{-1}. The inactive length is divided by the multiplicity to obtain the effective inactive length, which is the low-mass value of Fig. 18. The assumed error in the multiplicity then corresponds to an error of ± 0.11 g/cm² in the placement of the origin of the mass axis.

The confidence level for the straight-line fit is only 3% but the correction is small, only (3.8 ± 1.2) $\times 10^{-4}$. An additional error of 1.2×10^{-4} is assigned as a result of the uncertainty in the average multiplicity. Hence, the anti-counter mass correction

FIG. 17. Single-track plus multiple track NCC, ALL, and NCCSV events: Integrated charge asymmetry for all events in all bend-angle bins $\geq$ indicated abscissa.
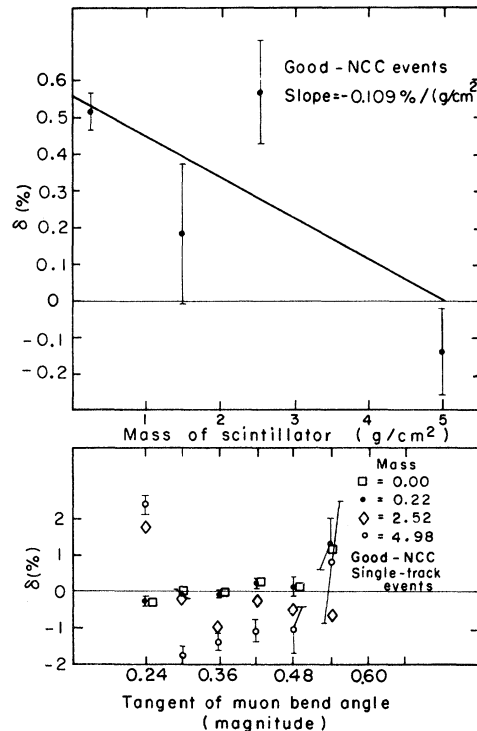

FIG. 18. Mass extrapolation when mass is placed downstream of the anti counters. (a) Charge asymmetry vs mass for the four mass points taken, with the best-fit straight line shown. The correction is (3.8 ± 1.2) $\times 10^{-4}$. (b) Charge asymmetry vs bend angle for the four mass points.

to the charge asymmetry is

$$\Delta\delta = (3.8 \pm 1.7) \times 10^{-4} \; .$$

Figure 18 also shows the charge asymmetry per bend-angle bin from 0.24 through 0.54 as a function of the anti-counter mass. This plot is useful because it shows the effect of a known source of neutron interactions in these bins. The plot substantiates the claim that the NCC events in these bins are free of neutrons, but that the CC events are not.

G. Knock-On Correction

Figure 19 illustrates the different ways in which a knock-on electron can affect an event. The 2-bin knock-ons are the type in which the electron merely causes a second bin to be on. However, due to the idiosyncrasies of the binning scheme, a knock-on can cause three bins to be on, or can shift the apparent muon position with or without the turning on of a second bin. A 3-bin knock-on can occur only if the real muon bin has two counters on; a shift of the muon position can occur only if the real muon bin has only one counter on.

The knock-on correction was studied both from the data and from the Monte Carlo events. Knock-ons were generated by the Monte Carlo according to the energy distribution given by Rossi.[16] The kinematic maximum knock-on energy was calculated separately for each muon. The minimum knock-on energy was taken to be 1 MeV. Fortunately, the magnetic field was so strong (6000 G)

that the calculation is very insensitive to this lower limit, which is not well known. Only 0.14% of the knock-ons which affected the muon track were less than 2 MeV.

The most important knock-on effect occurs in the R-bank, located near the middle of the magnet. Consider all NCC multiple-track events containing just two tracks with different R bins only. (Include the 3-bin configuration in Fig. 19.) This subsample represents 2.0% of the NCC data, and its net charge asymmetry before the neutron cut is very small, only $(1.1 \pm 0.3)\%$. Thus in the absence of the neutron cut, the charge asymmetry is similar to that of the total data. However, if the correlations between the two tracks are examined, it turns out that there are very large knock-on-type correlations. Thus, consider events in which one track is in bend-angle bin 0.30 and the second track is 3 bins displaced. If the second is in bin 0.48, the experimentally measured charge asymmetry is +45%; but if the second track is in bin 0.12, the measured charge asymmetry is -49%. This indicates that perhaps 45 to 50% of these events are knock-ons. Because the neutron cut is made in bin 0.24 and the criterion used was to choose the straightest track for all multiple-track events, a correction must be applied to account for the events which knock-ons place asymmetrically in the neutron cut. The approach taken is to assume that the entire charge asymmetry in the bin under consideration $[(45 \pm 2)\%$ in the above example] was due to knock-ons, and simply to add back the required number of events of the proper sign. The resulting corrections are shown in Table III for each bend-angle bin.

Similar studies were made for the Monte Carlo knock-on events, and the resulting predictions are also presented in Table III. The statistical errors of the Monte Carlo predictions are negligible com-
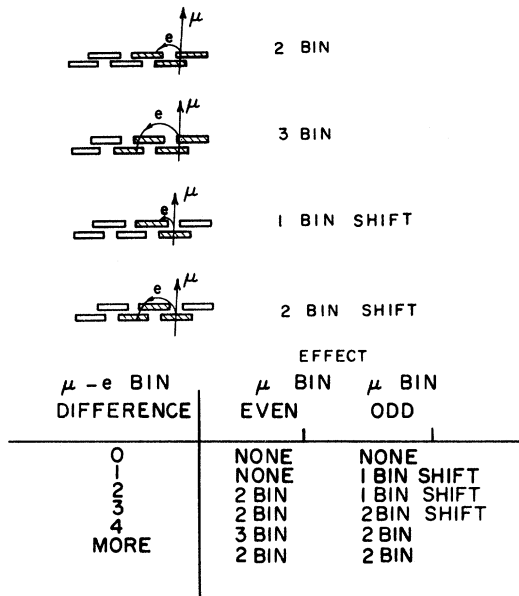
FIG. 19. The four types of knock-on electron processes which affect the charge-asymmetry measurement.

TABLE III. R knock-on corrections in terms of NCC asymmetric events.

| Bend-angle bin | Corrections | |
	Measured	Monte Carlo
0.24	2267	444
0.30	6235	4534
0.36	6093	6296
0.42	3293	3250
0.48	923	892
0.54	312	145
0.60	8	17
Total multiple track	19 131	15 578
1-bin-shift	4026	3536
Total	23 157	19 114
$\Delta\delta$ (%)	−0.558	−0.461

pared to the systematic error of about 10%. The measured corrections have no statistical error since they are direct measurements of the events concerned, if the above assumption of zero charge asymmetry in each bin except for knock-ons is justified. The agreement between Monte Carlo and measured corrections for bend angles ≥ 0.36 is excellent and instills confidence in the Monte Carlo predictions. However, the agreement near the neutron cut is poor and this disagreement will be the basis for the estimate of systematic error.

The 1-bin-shift knock-ons (Fig. 19) are especially troublesome since they do not indicate their presence with an extra track. They occur only when the muon goes through a single-counter (odd-numbered) R bin as shown in Fig. 19. Since they produce single-track events, they shift positive muons toward larger bend angles but negative muons toward smaller bend angles. A positive charge asymmetry of the even-numbered R bins in good-NCC events is caused by the shift of positive muons to an even bin, while the corresponding negative muons are lost in the neutron cut. Hence, by studying the events in the neutron cut the number of these lost negative muons can be measured. The measured 1-bin-shift knock-on correction in Table III is the difference of the asymmetric events with odd and even R bins in the neutron cut. The corresponding Monte Carlo correction is also listed.

The one-bin-shift R knock-ons play a major role in the determination of the charge asymmetry distribution (Fig. 15). The Monte Carlo predictions show that they approximately cancel the effects of the μ^+/μ^- range difference in the low-momentum bins of this plot and produce the relatively flat distribution. The total R knock-on corrections to the charge asymmetry from the data and Monte Carlo predictions are also given in Table III. The final R knock-on correction to the good-NCC events is taken to be the average of the two corrections. The systematic error is taken to be about half their difference:

$$\Delta\delta_{R \text{ knock-on}} = -(5.09 \pm 0.50)\times10^{-3} .$$

This correction is independent of the state of the C coincidence. The corresponding correction for good events is

$$\Delta\delta_{R \text{ knock-on (good)}} = -(5.01 \pm 0.50)\times10^{-3} .$$

The agreement of these two numbers shows that the the R knock-on correction is not influenced by the neutron-induced events.

The corrections for knock-ons in the S and T banks are much smaller than the R correction because the magnetic field was weak enough near the S and T banks so that most of the appropriate knock-ons were stopped by 1.2 cm of wood just downstream of these banks. These corrections are opposite in sign to the R correction. The measured corrections are

$$\Delta\delta_{S \text{ 1-bin-shift}} = +(1.7 \pm 0.4)\times10^{-4} ,$$

$$\Delta\delta_{T \text{ 1-bin-shift}} = +(2.4 \pm 0.4)\times10^{-4} ,$$

$$\Delta\delta_{S \text{ Multiple-track}} = +(1.4 \pm 0.4)\times10^{-4} ,$$

$$\Delta\delta_{T \text{ Multiple-track}} < 10^{-4} .$$

The correction for all knock-ons is then

$$\Delta\delta_{\text{all knock-ons}} = -(4.54 \pm 0.51)\times10^{-3} .$$

This correction restores the charge asymmetry nearly to its single-track value as might be expected.

We note here that the effects of extra tracks caused by strong interactions of pions are properly accounted for by the use of measured knock-on corrections. Specifically included in this statement are the effects of normal pions which scatter to the muon side and the effects of pions which interact before decay (thus before simulating a normal muon).

H. Randoms

Figure 20 illustrates some of the possible types of random events which might have been accepted. Type 1 represents the real events, and types 2 and 3 represent the random-trigger events which were continuously monitored through the use of delayed-time triggers. Correlated counts are joined by a line representing a particle's trajectory. Uncorrelated counts are not joined. Event-type 4 illus-

TABLE IV. Randoms subtractions for good-NCC events.

Type of events	Number of events	Asymmetric events	Asymmetries in %		
			δ	Λ	α
Prompt	4 224 279	26 904	0.64	−0.30	−0.04
Delayed W	43 861	3604	8.22	−5.68	−0.64
Delayed P	30 545	1892	6.19	−0.45	−0.04
Real	4 149 873	21 408	0.52	−0.25	−0.04

trates why randoms subtractions are notoriously unreliable. This type of event is included in the measurement of all of the first three types. Hence, when one subtracts the measured types 2 and 3 from 1, one subtracts type 4 twice. Events of type 4 cannot be measured by any randoms monitoring technique which uses two time slices. Since three time slices were actually used in this experiment, events of type 4 could be properly measured. However, there is an infinite number of randoms configurations which could not be measured. A randoms subtraction thus makes sense only if the beam intensity is sufficiently low that only a few of the many possibilities need to be considered. Fortunately, this was true for this experiment. The on-times of individual counters (the on-time is defined as the probability that a counter or counter configuration is on at a random point in time) were typically about 0.3%, and for all W bins combined the on-time was about 0.2%.

1. Measured Random Triggers

The randoms subtractions which have been made on the main data sample are listed in Table IV. The main problem involved in making the measurements was to ensure that prompt and delayed time slices were equivalent. Because the separation between time slices was precisely the time of one Bevatron revolution, beam structure was properly taken into account. Another consideration was to ensure that prompt and delayed time coincidence circuits had equal resolving times. This equality was established to within $\pm 5\%$ for all relevant circuits. Hence, it is believed that these randoms subtractions were measured to a systematic accuracy of $\pm 5\%$. Measured random triggers account for only 1.8% of the data, and thus the statistical error of the randoms subtraction is negligible (1% of δ). The correction for measured random-trigger events is

$$\Delta\delta = (-12.1 \pm 0.6)\times 10^{-4} .$$

2. Unmeasured Randoms

The main problem in making a randoms subtraction is knowing whether one is subtracting all of the necessary events. Since the R and T banks were generally not required in the trigger logic, events of types 5, 6, and 7 (Fig. 20) were correctly subtracted with the delayed W events. However, events of type 8, 11, and 14 would be correctly subtracted only if the S bank was not in the strobe. Such events were studied via the S time-to-pulse-height analyses. The contribution to the charge asymmetry of these random S events is

$$\Delta\delta_{[S]} = (0.3 \pm 1.4)\times 10^{-4} .$$

Events of types 9 and 10 satisfy requirements for a $K_{\mu3}^0$ signature which are only slightly less stringent than normal. The M counter randoms are charge symmetric, and random P counts must be charge symmetric because the P counters are upstream of the magnetic field. Hence, events of types 9 and 10 are accepted as $K_{\mu3}^0$.

The contribution to the charge asymmetry of type 4 events is 2×10^{-5}. This number was determined by multiplying the delayed P contribution (type 2) by the ratio of the asymmetric muon events of types $PSRT[W]/PSRTW$. Events with the pion P and muon W correlated in random time, such as event type 13, make a contribution to the charge asymmetry of less than 10^{-4}.

Hence, the randoms subtraction has performed the necessary correction to the charge asymmetry for random events to an accuracy of 2×10^{-4}. The error of the randoms subtraction is increased accordingly.

3. Single-Bin Randoms

The main effect of single-bin randoms is to shift the apparent muon position in a given bank in the same manner as accomplished by knock-ons (see Fig. 19). However, randoms are much less im-
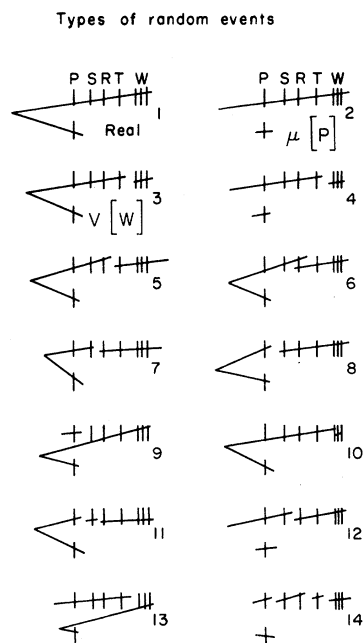
Types of random events

FIG. 20. Types of random triggers. Correlated counters are joined by a line representing a particle trajectory. Uncorrelated counts are not joined. Types 2 ($\mu[P]$) and 3 ($V[W]$) are directly measured by the electronic circuitry.

portant than knock-ons because they are not cor-
related with the muon track. For a given bank we
define:

Λ_i = geometrical bias of events in bin i,

$O_i^\dagger$ = on-time probability of bin i with the
field up.

Then a reasonable definition of the effective
charge of a random in bin i is Λ_i if the field is up
and $-\Lambda_i$ if the field is down. Hence, the on-time
for asymmetric randoms in bin i is given by
$\frac{1}{2}\Lambda_i(O_i^\dagger - O_i^\downarrow)$. The sum of the asymmetric on-times
(average of up and down) is found to be $(65 \pm 3) \times 10^{-4}$
for the T bank, and less than $(2 \pm 3) \times 10^{-4}$ for each
of the S, R, L, M, and N banks. As in the case of
knock-ons the main danger is that single-bin ran-
doms may shift the bend angle of events asymme-
trically into the neutron cut. Less than about 30%
of the randoms in an S, R, or T bank are close
enough to any particular muon track to affect its
bend angle. Hence, the above numbers indicate
that the effects of randoms in banks other than the
T bank are completely negligible. Using a method
similar to that employed in studying the R knock-
on correction, the effects in the T bank change the
charge asymmetry by less than 10^{-4}.

I. Pion Interactions

1. P-Counter Mass Extrapolation

The P mass extrapolation was performed in order
to measure the charge asymmetry in the absorp-
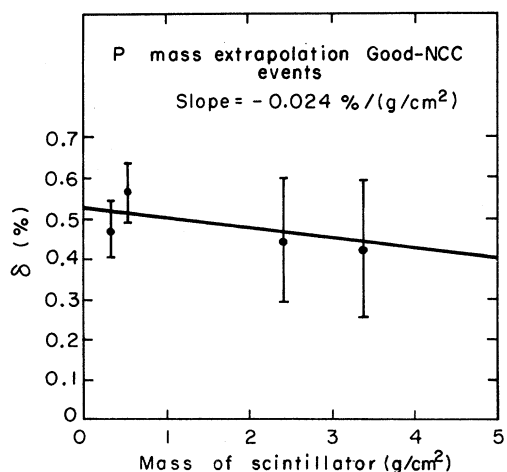tion of $K_{\mu3}^0$ pions before they could traverse the in-

P mass extrapolation Good-NCC
events

Slope = -0.024 %/(g/cm²)

FIG. 21. Mass extrapolation for mass placed up-
stream of the P counters (to absorb pions). The charge
asymmetry is shown for the four mass points, along
with the best-fit straight line. The correction is
$(0.9 \pm 3.6) \times 10^{-4}$.

active length of a P counter. The plot is shown in
Fig. 21. Differing amounts of wrapped scintillator
were placed upstream of P_{up} and P_{down} to provide
the two high-mass points. The two low-mass points
represent the portions of the main data with the
pion up and down. The two P counters were run
with different discrimination levels in order to pro-
vide these two points. The straight-line fit is good
and the correction is $\Delta\delta = (0.9 \pm 3.6) \times 10^{-4}$.

This correction is consistent with the assumption
that π^- charge-exchange scattering on the free hy-
drogen in scintillator is the only important cause
of π^+/π^- differential absorption in the system.
Apparently the system is insensitive to the final-
state differences of π^+ and π^- charge-exchange
scattering on carbon. The sensitivity to these fi-
nal-state differences cannot be calculated reliably,
and could be highly dependent on the experimental
configuration.

2. Penetration of Lead Wall

This section deals with the possibility that pions
penetrated the lead wall without decaying and were
thus identified incorrectly as muons. (Decay in
flight is considered in Sec. IV I 3.) Since this pene-
traction is a small effect, the main concern is that
pions may have penetrated the lead wall asymme-
trically.

One possible mechanism for this penetration is
the passage of pions through a portion of the hole
in the lead wall. Such events must register an H
count. Events with an H counter on comprise
5.3% of the data, of which 3.1% is due to H ran-
doms. The contribution of all H events to the
charge asymmetry is $(-2.7 \pm 1.1) \times 10^{-4}$. This con-
tribution is small but not negligible. However,
the H counts associated with this contribution are
not correlated with the W bins of their events.
Hence, this slight charge asymmetry is attributed
to interactions of pions from normal $K_{\mu3}^0$ events
which did not penetrate the lead wall. Consequent-
ly, no correction will be made for this effect.

The most direct route for pions to take to the L
bank is through the entire lead wall. It is known,
from the analysis described above, that some
strongly interacting particles (probably high-ener-
gy protons) are able to take this path. Since the
lead wall was only about five interaction lengths
thick (including steel plates), probably about 0.7%
of such protons passed through the wall without
having a strong interaction at all. The pions from
K_L^0 decay, however, are expected to have a much
smaller penetration probability, due to their lower
momenta and higher cross sections near the first
pion-nucleon resonance. One possible way of dif-
ferentiating these pion penetrations from the main

muon sample is to examine events with multiple W bins, because pions traversing lead at the end of their range can be expected to produce two or more high-energy spatially-separated tracks much more often than muons.

Calculations indicate that essentially all of the events with multiple W bins were due to muon knock-ons. Their measured asymmetry was small: In the good-NCC sample, the asymmetric events $(N_+ - N_-)$ numbered -476 ± 365. Assigning *all* of these events to asymmetric pion penetration, and assuming that $\frac{1}{3}$ of all penetrating pions were detected through the mechanism of multiple W bins, the estimated correction to the charge asymmetry is $(4 \pm 3) \times 10^{-4}$. The pion detection efficiency of $\frac{1}{3}$ is indicated by the measured detection efficiency for protons (identified by their charge asymmetry[3]). The difference in pion and proton inelastic cross sections on nuclei at the relevant incident energies has been taken into account, and increases the estimated pion detection efficiency by a factor of two over that measured for protons. Since the above correction is not statistically significant and is small relative to the final error of the experiment, no correction for pion penetration will be made. However, the fact that we cannot prove that this correction is less than 10^{-4} will be noted by its appearance in Table I.

3. Decay in Flight

A Monte Carlo calculation predicts that $(14 \pm 2)\%$ of the events are actually due to pion decay in flight. The mechanism is K_L^0 decay to a mode yielding two charged particles into the acceptance; one of these is a pion, which subsequently decays to a muon, which in turn penetrates the lead wall. The calculated contributions from various K_L^0 decay modes are shown in Table V.

The charge asymmetries of the pions in each decay mode are also listed in Table V. The K_{e3}^0 result is taken from Marx.[5] The asymmetry in $K_{\mu3}^0$ decay is the result of this experiment. These pion charge asymmetries change as the pions interact

TABLE V. Monte Carlo calculation of the contribution to δ from pion decay in flight after K_L^0 decay into $\pi e\nu$ (K_{e3}^0), $\pi\mu\nu$ ($K_{\mu3}^0$), and $\pi\pi\pi$ ($K_{\pi3}^0$).

Mode	Fraction of events (%)	Charge asymmetry after decay
K_{e3}^0	7.8	$-(3.22 \pm 0.29) \times 10^{-3}$
$K_{\mu3}^0$	5.4	$-(6.0 \pm 1.4) \times 10^{-3}$
$K_{\pi3}^0$	0.5	0
Total	13.7	

while traversing the system. The concern here is with penetration mechanisms in which the particle penetrating the lead wall is a muon. The only feasible way in which muons can be produced is from the decay in flight of π and K mesons. Since π^+ and π^- are isospin conjugates, only $\pi^\pm$ interactions with unpaired nucleons can cause an asymmetry in the number of $\pi^\pm$, and thus an asymmetry in $\mu^\pm$ after pion decay. However, this is *not* true if K^+ mesons are produced, because the isospin conjugate of the K^+ is the K^0, not the K^-.

The main cause of charge asymmetry in pion decay in flight is preferential absorption of one charge over the other. Extensive data exist on the π-nucleon cross sections.[17] The absorption cross section (σ_a) on a nucleon is taken to be the difference of the total and elastic cross sections. With this definition, it is found that $\sigma_a(\pi^- p) - \sigma_a(\pi^+ p) = 5 \pm 2$ mb for incident pions in the momentum range of interest (1.2–2.5 GeV/c). The mass in the path of the pions upstream of the T bank, for most of the data taking, consisted of 12.0 g/cm^2 of aluminum and 6.5 g/cm^2 of wood and scintillator (both taken to be CH). If the contribution to the charge asymmetry is calculated from pion interactions with the hydrogen nuclei, using the above cross section difference, it is found that $\Delta\delta = 6 \times 10^{-5}$. The corresponding calculation for the unpaired neutron in each aluminum nucleus yields $\Delta\delta = -5 \times 10^{-5}$. Pion interactions in the lead wall and steel plate near the T counters produce similarly small changes in the charge asymmetry. K^+ associated production followed by $K_{\mu2}^+$ decay is completely asymmetric but the relevant K^+ production cross sections are small.[18] The change in the charge asymmetry is again negligible (5×10^{-5}). Therefore, the correction for the asymmetric events caused by decay in flight is entirely due to the CP-violating asymmetry in $K_{\mu3}^0$ and K_{e3}^0. The correction is $\Delta\delta = +(5.7 \pm 1.0) \times 10^{-4}$.

Because decay in flight accounts for a significant fraction of the data, an additional correction must be made after all other corrections to compensate for the dilution of the charge asymmetry by decay in flight.

J. Muon Interactions

1. $\mu^\pm$ Range Difference

The range difference between μ^+ and μ^- has recently been calculated.[19] This calculated difference is in agreement with recent measurements[20] made with a lead, carbon, and iron absorber to an accuracy of about 10%. According to the theory, for incident momenta of interest in this experiment (1.1–1.5 GeV/c) the range difference ΔR

$\equiv R_- - R_+$ varies linearly with the range R such that $\Delta R/R$ is nearly constant at about 2×10^{-3}. The value of $\Delta R/R$ is nearly independent of the absorber material at these incident momenta.

The range-difference correction is a major one in this experiment. The important question to be answered is how many μ^- successfully counted in the M bank while the corresponding μ^+ stopped short of counting. The correction to the charge asymmetry is

$$\Delta\delta = \frac{1}{2n} \frac{dn}{dR} \Delta R \; ,$$

where n is the total number of events detected and $\frac{1}{2}dn$ is the number of μ^- stopping in dR at R. The average incident momentum of muons which stopped near the M bank was determined to be 1290 ± 35 MeV/c by the Monte Carlo calculation (which succeeds in predicting the average momentum of the total muon sample – see Fig. 11). Assigning a 4% accuracy to the range-difference theory in calculating ΔR for the muons of interest we find

$$\Delta R = 1.63 \pm 0.08 \text{ g/cm}^2 \text{ of iron.}$$

However, the major source of error in the range-difference correction is lack of precise knowledge of the muon-stopping distribution. Since the N bank was not required in the $K^0_{\mu3}$ signature, we were able to measure that 0.293 ± 0.004 of the accepted muons either stopped in the last steel plate or missed the N bank. The Monte Carlo prediction for this number was 0.265 ± 0.006, where the statistical error of the Monte Carlo calculation has been indicated. Hence the prediction was correct to a systematic accuracy of 10%. The Monte Carlo prediction was then used to extrapolate this measured value of $\Delta n/n$ for the whole steel plate to the value of

$$\Delta\delta = (31 \pm 7) \times 10^{-4}$$

for the μ^- stopping in the first 1.63 g/cm² of the plate. We note from Fig. 10 that the Monte Carlo prediction successfully describes the multiple scattering in the lead wall.

2. End-of-Range Differences

Positive and negative muons behave differently at the end of their range. For this correction the most important muons are those which stopped in the 5 cm steel plate between the L and M counters, but originated from a $K^0_{\mu3}$ decay satisfying all upstream $K^0_{\mu3}$ signature criteria. The ratio of the number of such muons to the number of muons associated with events which passed all signature criteria is 0.30 ± 0.03 according to the Monte

TABLE VI. x rays of muons captured in iron.

x ray	Energy (MeV)	Relative intensity
K_α	1.26	0.71
K_β	1.53	0.08
K_ν	1.70	0.21

Carlo prediction. Secondaries associated with the muons which stopped in this plate could have reached the M bank, thereby completing the signature requirements. A bias on the charge asymmetry results from asymmetrical completion of these requirements.

When a μ^+ stops in the above plate, it decays to an e^+ with a lifetime of 2.2 μsec.[21] A μ^-, however, cascades into the lowest Bohr orbit around an iron nucleus, where it is subject to capture as well as decay. The decay probability of the μ^- in a bound state is nearly the same as that of a free muon.[22] However, due to the large capture probability, the lifetime of a μ^- in the first Bohr orbit about an iron nucleus is only 200 nsec.[23] The net effect of μ^+ decaying to e^+ is negligible. The main bias on the charge asymmetry caused by end-of-the-range effects is due to μ-mesonic x rays produced during the cascade into the first Bohr orbit for iron. Essentially all μ^- that are stopped produce such an x ray well within the 15-nsec sensitive time.[24] (This 15 nsec sensitive time is that part of the full 60 nsec resolving time which was present *after* the main timing peak for stopping muons in the M counters. The remaining 45 nsec was before the main peak. This asymmetrical timing arrangement was necessary to eliminate an extremely small dead time.) The energies and relative intensities of these x rays are listed in Table VI.[25] (Here K_α, K_β, K_ν refer to the $2P \to 1S$, $3P \to 1S$, and $nP \to 1S$ transitions, where $n > 3$.) The efficiencies for detecting these x rays in the M counters were calculated from the Klein-Nishina formula as given by Rossi.[26] The main source of uncertainty in this calculation is lack of exact knowledge of the threshold of the M counters. This average threshold was determined to be 0.8 ± 0.1 MeV from the known pulse heights for minimum-ionizing particles. The detection efficiency for the K_α x ray is particularly sensitive to this threshold value. The absorption lengths of the cascade x rays in iron were also calculated from the Klein-Nishina formula. The results of the calculations are presented in Table VII. The total correction to the charge asymmetry from cascade x rays is then

$$\Delta\delta_{\text{x rays}} = +(3.94^{+0.96}_{-1.45}) \times 10^{-4} \; .$$

TABLE VII. Corrections due to x rays after muon capture in iron.

x ray	(In %) detection efficiency	Fraction of μ with γ reaching M bank (%)	Correction $\Delta\delta$ (10^{-4})
K_α	$1.3^{+0.2}_{-0.6}$	1.50 ± 0.30	$1.95^{+0.49}_{-0.98}$
K_β	2.2 ± 0.3	0.20 ± 0.04	0.44 ± 0.11
K_ν	2.8 ± 0.3	0.55 ± 0.11	1.55 ± 0.36

The mean numbers of γ rays[27] and neutrons emitted from an iron nucleus after μ^- capture are not well known. The absorption length of a neutron (3–30 MeV) in iron is about the same (35 g/cm^2) as the absorption length for a 1.5-MeV γ ray, but the detection efficiency for such neutrons in the M bank is only about 0.7%. A reasonable assumption is that about 1 neutron and about 1 γ ray are emitted after each μ^- capture. This is the equivalent of about 1.3 γ rays. A correction for secondaries emitted from the nucleus after μ^- capture would then be

$$\Delta\delta \simeq 1.3 \times \frac{15 \text{ nsec}}{200 \text{ nsec}} \times 3.9 \times 10^{-4} = 4 \times 10^{-5} .$$

This correction is negligible, but in order to take its uncertainty into account we symmetrize the error of the correction for x rays:

$$\Delta\delta_{\text{end-of-range}} = +(3.9 \pm 1.5) \times 10^{-4} .$$

V. SUMMARY

The $K_{\mu 3}^0$ charge asymmetry is determined as shown in Table I. The systematic errors are to be interpreted as one standard deviation. Since the correlations among the corrections are believed to be insignificant, the errors are combined in quadrature to yield

$$\delta = (6.0 \pm 1.4) \times 10^{-3} .$$

ACKNOWLEDGMENT

*Present address: Department of Physics, State University of New York, Stony Brook, New York 11790.

†Present address: Department of Physics and Astronomy, University of Tel-Aviv, Tel Aviv, Israel.

‡Present address: Department of Physics, Northwestern University, Evanston, Illinois 60201.

§Present address: Department of Biological Sciences, Columbia University, New York, N. Y. 10027.

[1] The neglect of electromagnetic final-state interactions has been discussed by C. Ryan, Phys. Rev. D $\underline{1}$, 299 (1970). Our detection efficiency was not uniform over the Dalitz plot but was weighted toward high muon and pion energies in the K meson rest frame. Hence this assumption may not be valid if CP violation occurs in the electromagnetic interaction.

[2] $x_l = \langle \pi^- l^+ \nu | H_w | \overline{K}^0 \rangle / \langle \pi^- l^+ \nu | H_w | K^0 \rangle$. The phase of x_l is defined by the fact that $|K_2^0\rangle = (|K^0\rangle - |\overline{K}^0\rangle)/\sqrt{2}$ has $CP = -1$. The definition of x_l can be generalized to include dependence on the Dalitz plot parameters and lepton helicities; see L. M. Sehgal, Phys. Rev. Letters $\underline{21}$, 412 (1968).

[3] This experiment is discussed in greater detail by R. L. McCarthy, Ph.D. thesis, University of California, Berkeley, available as Lawrence Berkeley Laboratory Report No. LBL-550, 1971 (unpublished). Also, R. L. McCarthy $et\,al.$, Phys. Letters $\underline{42B}$, 291 (1972).

[4] M. A. Paciotti, Ph.D. thesis, University of California, Berkeley, available as Lawrence Radiation Laboratory report No. UCRL-19446, 1970 (unpublished). This is a reanalysis of the data of D. Dorfan $et\,al.$, Phys. Rev. Letters $\underline{19}$, 987 (1967). We have used the prescription in Paciotti's thesis (p. 56) to correct for the range differences between μ^+ and μ^-.

[5] J. Marx $et\,al.$, Phys. Letters $\underline{33B}$, 222 (1970).

[6] The superweak theory as presented by T. D. Lee and L. Wolfenstein, Phys. Rev. $\underline{138}$, B1490 (1965), predicts $\epsilon = \eta_{+-} = \eta_{00}$ and $\arg\epsilon = \tan^{-1}(2\Delta m \tau_S)$. Hence $2\text{Re}\epsilon = 2|\eta_{+-}|\cos(\arg\epsilon)$. We take $|\eta_{+-}| = (1.91 \pm 0.06) \times 10^{-3}$ from V. Fitch $et\,al.$, Phys. Rev. $\underline{164}$, 1711 (1967). We also take $\tan^{-1}(2\Delta m \tau_S) = 43.2° \pm 0.4°$ from S. H. Aronson $et\,al.$, Phys. Rev. Letters $\underline{25}$, 1057 (1970).

[7] S. Bennett $et\,al.$, Phys. Letters $\underline{29B}$, 317 (1969).

[8] $\text{Re}(x_\mu) = 0.19^{+0.13}_{-0.18}$ and $\text{Im}(x_\mu) = -0.12^{+0.20}_{-0.17}$ from B. Webber $et\,al.$, Phys. Rev. D $\underline{3}$, 71 (1971). Also, $\text{Re}(x_\mu) = 0.04^{+0.10}_{-0.13}$ and $\text{Im}(x_\mu) = 0.12^{+0.17}_{-0.16}$ from M. F. Graham $et\,al.$, Nuovo Cimento $\underline{9A}$, 166 (1972).

[9] R. M. Graven $et\,al.$, Nucl. Instrum. and Methods $\underline{102}$, 45 (1972).

[10] L. Okun', Ann. Rev. Nucl. Sci. $\underline{9}$, 89 (1959).

[11] R. P. Johnson, private communication. The apparatus used for this measurement is discussed in A. R. Clark $et\,al.$, Phys. Rev. Letters $\underline{26}$, 1667 (1971).

[12] The angular dependence was assumed to be
exp(−3.9$P\theta$), where P is the K_L^0 momentum in GeV/c,
and θ is the production angle, as given by G. Trilling,
Lawrence Radiation Laboratory Report No. UCRL-16830
(unpublished), Vol. 1, p. 38.

[13] B. Rossi, *High Energy Physics* (Prentice-Hall,
Englewood Cliffs, New Jersey, 1952), p. 32.

[14] This definition is in accord with J. Marx *et al.*, Ref. 5.

[15] M. N. Kreisler, Ph.D. dissertation, Stanford University, 1966 (unpublished), p. 83.

[16] B. Rossi, Ref. 13, p. 16.

[17] See, for example, G. Giacomelli, P. Pini, and
S. Stagni, CERN Report No. CERN/HERA 69-1., 1969

(unpublished).

[18] O. I. Dahl *et al.*, Phys. Rev. 163, 1430 (1967).

[19] J. D. Jackson and R. L. McCarthy, Phys. Rev. B 6, 4131 (1972).

[20] A. R. Clark *et al.*, Phys. Letters 41B, 229 (1972).

[21] A. O. Weissenberg, *Muons* (North-Holland, Amsterdam, 1967), p. 15.

[22] A. O. Weissenberg, Ref. 21, p. 177.

[23] A. O. Weissenberg, Ref. 21, p. 163.

[24] C. S. Johnson *et al.*, Phys. Rev. 125, 2111 (1962).

[25] D. Quitmann *et al.*, Nucl. Phys. 51, 609 (1964).

[26] B. Rossi, Ref. 13, p. 78.

[27] A. O. Weissenberg, Ref. 21, p. 175.

Production of K_L^0 Mesons and Neutrons from Electrons on Beryllium Above 10 GeV*

G. W. Brandenburg, A. D. Brody, W. B. Johnson, D. W. G. S. Leith, J. S. Loos,† G. J. Luste,‡
J. A. J. Matthews, K. Moriyasu,§ B. C. Shen, ‖ W. M. Smart,** F. C. Winkelmann, and R. J. Yamartino
Stanford Linear Accelerator Center, Stanford University, Stanford, California 94305
(Received 14 August 1972)

Measurements are presented of the yields of K_L^0 mesons and neutrons produced by electrons of energies between 10 and 19 GeV incident on 0.70- and 1.75-radiation-length beryllium targets for production angles between 1.6° and 4°. Values for the K_L^0 absorption cross section on lead are also found for momenta between 1.4 and 7.4 GeV/c. A successful interpretation of K_L^0 production is made in terms of the process $\gamma N \rightarrow K_L^0 X$, where X represents an inclusive sum over all final states. The invariant structure function for K_L^0 photoproduction, extracted from the Be yields, is found to be simply related to the result for hydrogen by an over-all multiplicative factor, A_{eff}, the effective number of nucleons in the target nucleus. The results of the theoretical analysis are also compared to charged-K photoproduction and extrapolated to electron energies of 50 GeV.

I. INTRODUCTION

We present measurements of the yield of K_L^0 mesons and neutrons produced from electrons incident on a beryllium target at energies between 10 and 19 GeV. Table I summarizes the specific electron energies, production angles, and Be target thicknesses for which these measurements have been made. The data were acquired during three separate data runs at the Stanford Linear Accelerator Center (SLAC) in which the SLAC 40-in. hydrogen-filled bubble chamber was exposed to a neutral beam. A description of the neutral beam is given in Sec. II. A preliminary report of the results for run I is given in Ref. 1. Measurements of K_L^0 photoproduction below 10 GeV on complex nuclei have also been made in other experiments.[2-5]

The yields of K_L^0 and neutrons are presented in Secs. III and IV, respectively. The yields are found to behave similarly above ~4 GeV/c, where both show a rapid falloff with increasing momen-

tum of the neutral particle. However, for momenta below ~2 GeV/c the neutron yield has an intense low-energy component which is not present in the K_L^0 yield. This low-energy component is probably due to the disintegration of the target nucleus.

The present measurements of K_L^0 yields, together with previous measurements,[1-3] suggest that the photoproduction of K^0 mesons is a complicated process with contributions not only from the obvious two-body and quasi-two-body reactions but also from multiparticle channels. A natural framework for dealing with such a complicated situation is provided by the inclusive single-particle production process, $\gamma N \rightarrow K_L^0 X$, where X represents the sum of all final-state configurations. In Sec. V, we discuss the K_L^0 yields in terms of inclusive K_L^0 production and find a satisfactory description for the measurements. Extrapolations are then made for K_L^0 yields at higher energies and for various target thicknesses. Comparisons are also made to the available yield data for K^+ and K^- mesons.